

Analysis on Stitched Mode I Specimen Using Spring Elements

Jonathan Tapullima*, Hyung Woo Sim*, Jin Hwe Kweon*, Jin Ho Choi*[†]

ABSTRACT: Several studies related to reinforce composites structures in the through thickness direction have been developed along the years. As follows, in this study a new reinforced process is proposed based on previous experimental results using a novel stitching process in T-joints and one-stitched specimens. It was established the need to perform more analysis under standard test methods to obtain a better understanding. FEM analysis were compared after performed mode I interlaminar fracture toughness test, using different stitching patterns to analyze the through thickness strength with reference laminates without stitching. The stitching patterns were defined in 2×2 and 3×3 , where the upper and lower head of the non-continuous stitching process (I-Fiber) has proven to influence in a higher through thickness strength of the laminate. In order to design the numerical model, cohesive parameters were required to define the surface to surface bonding elements using the cohesive zone method (CZM) and simulate the crack opening behavior from the double cantilever beam (DCB) test.

Key Words: I-fiber, Stitching, DCB (Double Cantilever Beam), CZM (Cohesive Zone Method), Interlaminar Fracture Toughness

1. INTRODUCTION

The development of composite structures is strongly associated with joining methods. Usually, metal structures such as skins and stiffeners are mechanically assembled using rivets or bolts, because these have very good structural reliability owing to their low rate of defects as isotropic materials. However, it is difficult to apply these mechanical joints to composite materials, because fastener holes can break fibers and cause local delamination and cracks in the material's matrix [1]. Therefore, several methods have been developed to increase the through-thickness strength of bonded joints, such as stitching, braiding, tufting, weaving, and z-pinning; all these methods have been studied with the goal of identifying the best method for structure reinforcement [2-7].

When a delamination crack reaches the reinforcement, the crack's tip is protected by the bridging force, which persists even after the crack has propagated several millimeters further. This bridging effect decreases the crack's force, dissipating further crack propagation and therefore increasing the delami-

nation resistance [8]. The relationship between the force applied by the reinforcement and the cracked surface separation is described by the bridging law. The component along the direction of opening is usually referred to as mode I [9,10].

Hence, a novel stitching technique was developed to increase the strength of laminated composites in the thickness direction [11]. The capacity to ensure significant improvement in the delamination resistance shows the advantage of this new technique, which is called the I-Fiber stitching method. The stitching process was developed by designing an in-house build automatic stitching machine, which was used in this study.

To design a numerical model, the cohesive zone method (CZM) was used to simulate the crack-opening delamination behavior from the DCB test. Several studies have predicted the mechanical properties of Mode I in reinforced composite laminates, commonly using z-pin with various types of materials. In order to simulate the crack opening, cohesive elements are widely used; however, the methods to define the reinforcement can vary, for example Song *et al.* [12] used bilinear cohe-

Received 18 February 2019, received in revised form 30 April 2019, accepted 1 May 2019

*Research Center for Aircraft Parts Technology, School of Mechanical and Aerospace Engineering, Gyeongsang National University

[†]Research Center for Aircraft Parts Technology, School of Mechanical and Aerospace Engineering, Gyeongsang National University, Corresponding author (E-mail: choi@gnu.ac.kr)

sive elements to define the delamination and non-linear spring elements to define reinforcement in the composite laminate.

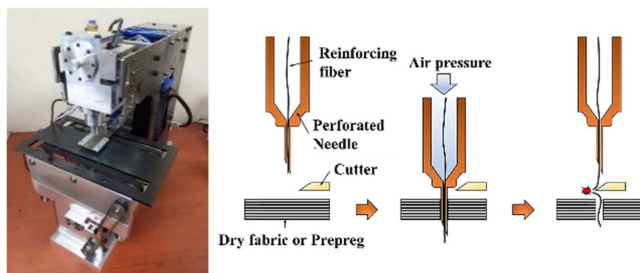
This study tested double cantilever beam (DCB) specimens with different stitched patterns, and observed their crack initiation and propagation mechanisms to understand the interlaminar resistance tendency of this new method. The results of this study indicated improvement in the materials' through-thickness properties; nevertheless, more exhaustive studies are underway.

2. EXPERIMENTAL PROCEDURE AND RESULTS

2.1 Manufacturing of test specimens

The stitching process has been developed using an in-house built automatic stitching machine. The stitching process starts with the insertion of a needle in the prepreg and the reinforcing fiber through it with air pressure. Finally, the needle is extracted to cut the stitched fiber and continue with the following stitching. The final step defines the name of this new method, the discontinuity in the stitching explains the I-fiber, where the remained stitched fiber on the top and bottom of the laminate create the "head" of the I-fiber. Fig. 1(a) shows the in-house built automatic stitching machine and Fig. 1(b) shows the schematic of the new stitching process.

The stitched specimens were divided into stitching patterns of 2×2 and 3×3 . A total of three cases were tested between no stitched specimen (reference case) and stitched specimens. The specimen thickness was 4.8 mm for all cases, and their lengths and widths were 150 mm and 25 mm, respectively. The initial length delamination was 50 mm, defined from the loading line to the crack tip. Following the ASTM D5528-01, two loading blocks with the dimensions of $25 \times 30 \times 16 \text{ mm}^3$ were attached to the specimens for performing the DCB test (Fig. 2(a)). The first stitching row was located at 6 mm from the crack tip for all of the cases, distributed in an area of 600 mm^2 . Different spacing was chosen for 2×2 and 3×3 patterns, to maintain symmetry in the both testing cases (Fig. 2(b)). The specimens were prepared using 40-ply with USN-125B (SK Chemicals), with stacking sequence $[0/45/90/-45/0]_{4S}$ and stitching yarn T300 6K [13] (Toray Industries, Inc).



(a) Automatic stitching machine (b) New stitching process

Fig. 1. Stitching machine design and process detail

Table 1. USN-125B material properties

Elastic Modulus (GPa)	E_1	141
	E_2	8.4
	E_3	8.4
Shear Modulus (GPa)	G_{12}	5.34
	G_{13}	5.34
	G_{23}	3.06
Poisson's Ratio	ν_{12}	0.298
	ν_{13}	0.298
	ν_{22}	0.47
Thickness (mm)	t	0.12

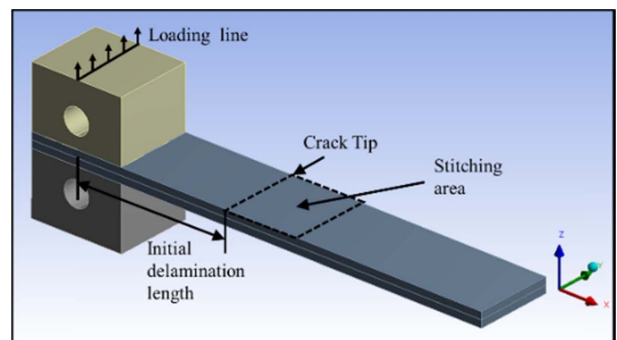
Table 2. TORAY T300 6K (fiber properties)

Elastic Modulus (GPa)	E_1	230
Tensile Strength (MPa)	σ_x	3530
Filament Diameter (μm)	T_f	7
Tensile Strain		1.5%
Density (g/cm^3)		1.76

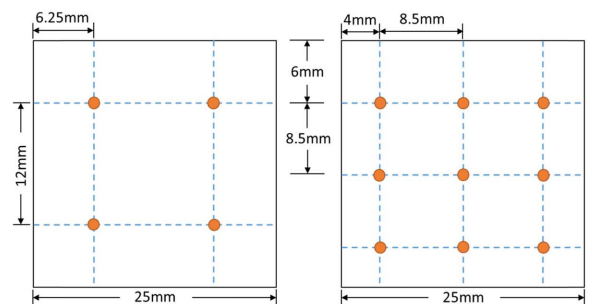
The properties of the carbon prepreg and stitched fiber are listed in Tables 1 and 2, respectively.

2.2 DCB test and experimental results

Following the ASTM indication to calculate the interlaminar fracture toughness and strain energy release rate (G_c), a printed ruler was bonded on one side of the specimen to mea-



(a) Configuration of DCB specimen

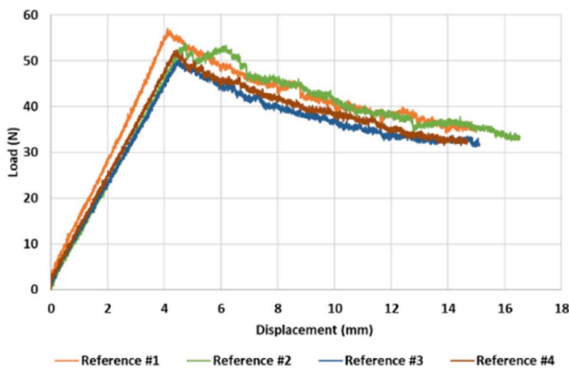


(b) 2×2 and 3×3 pattern distribution

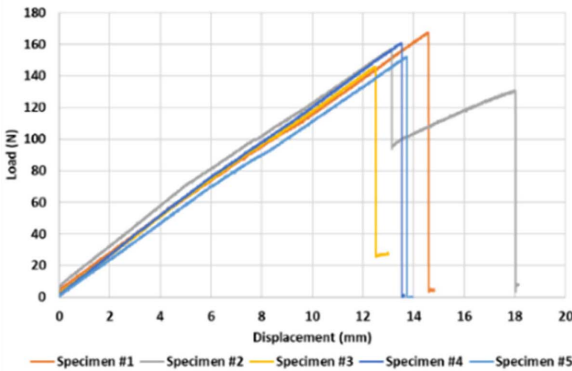
Fig. 2. DCB specimen and stitching patterns

sure the crack opening of the specimen during the test. The equipment used for the experiment was an INSTRON 5582 (Instron Co.) testing machine with 100 kN of loading capacity. The experiment was performed with a cross-head speed of 2 mm/min for all of the cases.

The obtained load-displacement curves for each case are shown in Fig. 3. From Figs. 3(b), 3(c), it is observed that when the stitched fibers are broken, the load-displacement curve abruptly drops and then rises again when there is a following stitch row. The 3 × 3 pattern specimen with a 3 mm head (Fig. 3(c)) exhibits the highest average failure load in the first stitched row with 201.53 N, and the largest displacement before failing completely; however, not all the tested specimens



(a) Not stitched



(b) Stitched 2×2 pattern

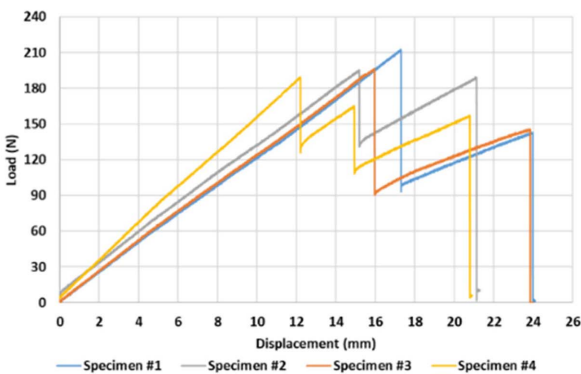


Fig. 3. Force-displacement curves of the DCB specimens

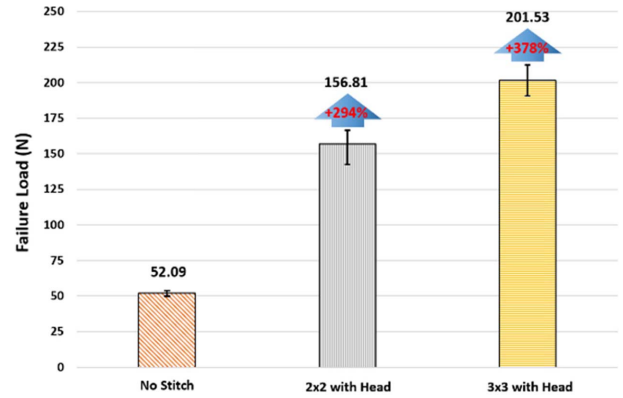


Fig. 4. Average ultimate failure loads, for all experiment cases

reach the third stitched line before a complete interlaminar failure.

The average ultimate failure loads of the DCB specimens for each case were calculated and are shown in Fig. 4. The failure load of the 3 × 3 pattern specimen with a 3 mm head was 378% larger than the specimen without stitching, which shows that the reinforcement effect of the I-fiber stitching process is outstanding.

3. SIMULATION METHODOLOGY

3.1 CZM

For the purpose of this work, is important to define Mode I as the main tensile stress test that describes debonding for the normal separation of the crack opening. Therefore, the traction-separation law with bilinear behavior proposed by Alfano and Crisfield [14] was chosen to simulate the experimental test, and the bilinear CZM was found to be more suitable for interfacial delamination (Fig. 5). This formulation has been defined with surface to surface cohesive elements, which allows to describe Mode I analysis as a debonding interface behavior. This fracture mechanism occurs when the adhesive (resin matrix) stops sticking to the adherent (laminate), and the mechanical forces that hold the bond together are broken by an external force [15].

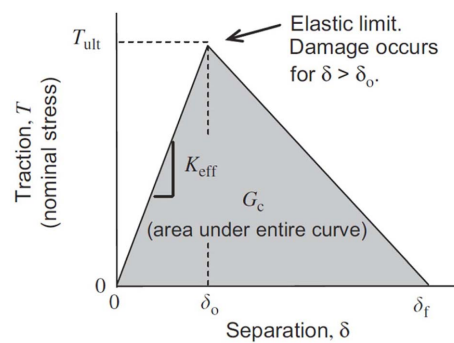


Fig. 5. Bilinear behavior proposed by Alfano and Crisfield

Table 3. Strain energy release rate calculation from experimental data

Ref 01	Ref 02	Ref 03	Ref 04	Average
0.217	0.193	0.203	0.199	0.203 mJ/mm ²

Three main characteristic parameters are needed to define the bilinear traction-separation relationship: the critical energy release rate (G_c), the maximal normal contact stress (T), and the stiffness (K). However, the only parameter that can be obtained from experimental tests is G_c , as shown in Table 3. Normal stress can be set after several iterations for the solution's convergence, and the stiffness is regarded as "default" by the numerical solver [16].

3.2 No stitched laminate DCB model

As was explained above, the cohesive elements were defined by the bilinear traction-separation law, which is characterized by K , T and G_c . The T value was defined after fit the ultimate failure load between the simulation and the no stitched experimental data (reference), in order to simulate an accurate response during the delamination. After several iterations, these parameters were set to: $T = 1.2$ MPa and $G_c = 0.20$ mJ/mm²; the value of K was a default value defined by the solver [17]. Fig. 6 shows the iterations before set the maximal normal contact stress T . To reduce the computational complexity, half of the model was considered in this study and constrained as required.

3.3 Stitched laminate DCB model

To define the numerical model of the stitched fiber, several studies were analyzed. The most studied cases are related to the z-pinning reinforcement, where the pin material can be a steel or carbon rod. Kravchenko *et al.* [18] performed a numerical Mode I analysis using carbon rods, which were characterized by non-linear spring elements from the load-displacement curve obtained from a single reinforcing element pull-out test. Bianchi *et al.* [19] and Mohamed *et al.* [20]

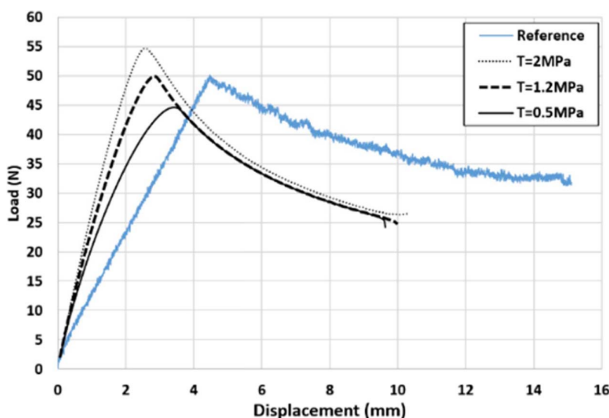


Fig. 6. No stitching laminate modeling

reported numerical analysis of reinforced laminates under Mode I for steel and carbon rods, respectively. Both groups developed CZMs, to define the response of the pinned elements using the traction-separation law.

This study analyses the stitched condition using linear spring elements. The longitudinal stiffness (K_s) of the spring element was calculated after several iteration in order to fit the slop with the experimental results. The propagation of the load-displacement curve from the FEM analysis was stopped after the spring elements strength reach the ultimate failure load obtained from the experiment. This method was able to approximate the numerical analysis for the FEM models in each stitched row. After several iterations, the longitudinal

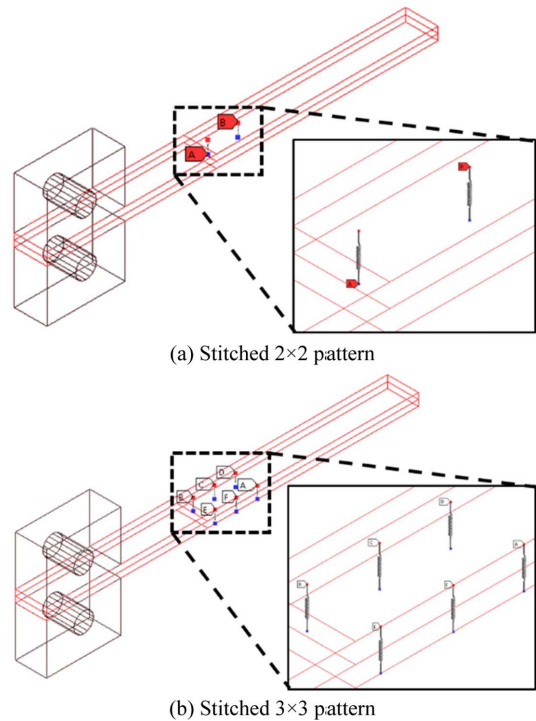


Fig. 7. Spring element distribution for FEM analysis using symmetric models

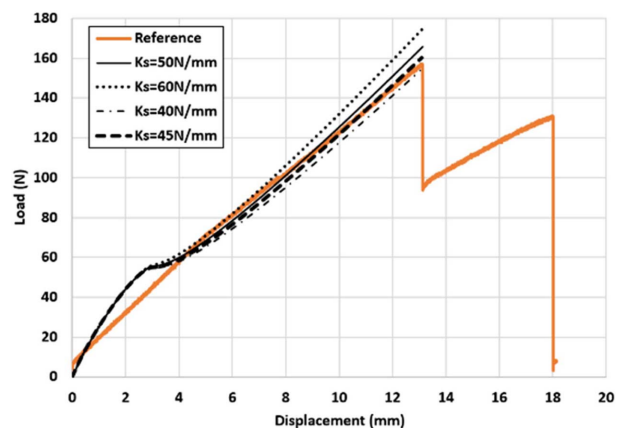


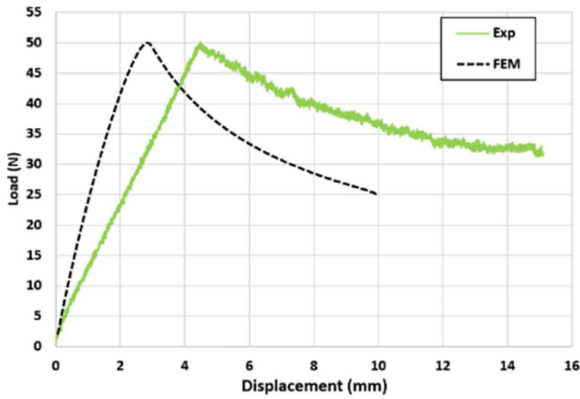
Fig. 8. Longitudinal Stiffness calculation

stiffness for all stitching cases was set to: $K_s = 45 \text{ N/mm}$. Fig. 7 shows the spring element distribution in the models for the stitching cases meanwhile Fig. 8 shows different values of K_s in order to fit the best value for an accurate comparison.

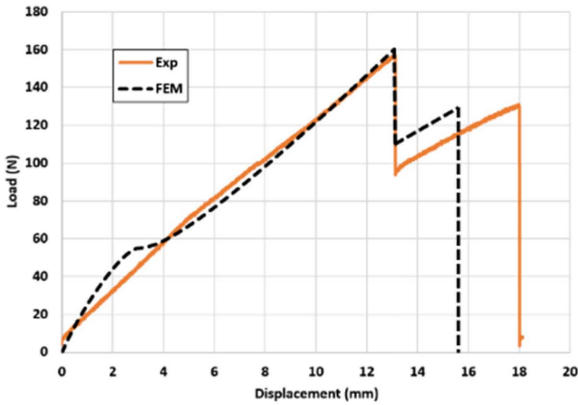
4. NUMERICAL RESULTS

4.1 Summary of FEA Results

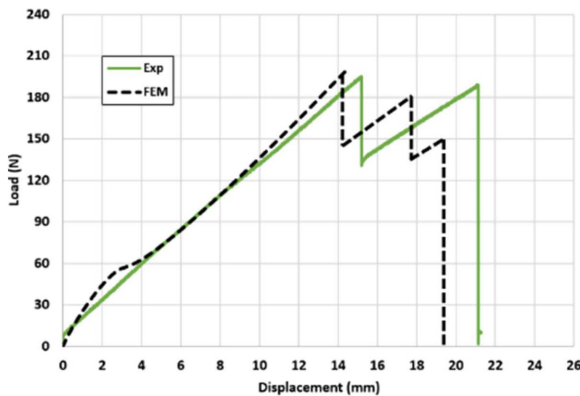
This section presents the results obtained for each simula-



(a) Non-stitched reference case



(b) Stitched 2×2 pattern



(c) Stitched 3×3 pattern

Fig. 9. DCB simulation results

tion case, and compares the FEM results with the corresponding experimental results. Fig. 9 shows all of the results for the three studied cases. Fig. 9(a) shows the reference case for the non-stitched laminate, for which after several iterations the maximal traction was calculated to define the parameters needed for the cohesive zone.

Fig. 9(b) shows the results for the 2×2 stitching pattern, it is possible to observe a similar tendency with the same maximal failure loads as the experiment. Finally, the result for the 3×3 pattern shows the higher maximal failure load compared with other experimental results and with similar tendency in the overall behavior. It is possible to appreciate the three peak reached in the FEM results due to the stitching pattern distribution before the final failure.

5. CONCLUSIONS

The 2×2 and 3×3 pattern tests demonstrated the improvement of the maximal load with the increment of the stitching fibers. The improvement of Mode I properties, obtained using this novel stitching method with respect to the reference specimens, reached a maximal average of 378%. The I-fiber head helped to avoid the complete pull-out by bonding the stitched fiber's head to the composite. Compared with other reinforcement methods, no complete pull-out was observed, and the failure load increased significantly in the z-direction.

In the same way, simulations showed the same tendency using the CZM to define the debonding parameters. Several iterations were required in order to obtain the same behavior as in the experimental results. The longitudinal stiffness was also defined to obtain an accurate approximation between FEM analysis and the experimental results for the stitching cases. Overall, these preliminary results indicate that the I-fiber stitching method is an outstanding candidate for effective reinforcement of composite structures in the through-thickness direction.

ACKNOWLEDGEMENT

This work was supported by the National Research Foundation of Korea (NRF) Grant funded by the Ministry of Science, ICT & Future Planning (NRF-2017R1A5A1015311).

REFERENCES

1. Ji, H., Kweon, J.H., and Choi, J.H., "Fatigue Characteristics of Stainless Steel Pin-reinforced Composite Hat Joints," *Composite Structures*, Vol. 108, 2014, pp. 49-56.
2. Jones, R.M., *Mechanics of Composite Materials 2nd edition*, Taylor & Francis Inc., 1999.
3. Mouritz, A.P., Bannister, M.K., Falzon, P.J., and Leong, K.H., "Review of Applications for Advanced Three-dimensional Fibre Textile Composites," *Composites Part A*, Vol. 30, 1999, pp.

- 1445-1461.
4. Ayranci, C., and Carey, J., "2D Braided Composites: A Review for Stiffness Critical Applications," *Composite Structures*, Vol. 85, 2008, pp. 43-58.
 5. Chou, S., and Chen, H.E., "The Weaving Methods of Three-dimensional Fabrics of Advanced Composite Materials," *Composite Structures*, Vol. 33, 1995, pp. 159-172.
 6. Chi, H., Li, Y., Koussios, S., and Beukers, A., "Bridging Micro-mechanisms of z-pin in Mixed Mode Delamination," *Composite Structures*, Vol. 93, 2011, pp. 2685-2695.
 7. Ko, F.K., *Three-dimensional Fabrics for Composites*, Composite Materials Series. Amsterdam: Elsevier Science, 1989.
 8. Grassi, M., and Zhang, X., "Finite Element Analyses of Mode I Interlaminar Delamination in z-fibre Reinforced Composite Laminates," *Journal of Composites Science and Technology*, Vol. 63, No. 12, 2003, pp. 1815-1832.
 9. Kang, M.S., Jeon, M.H., Kim, I.G., and Woo, K.S., "The Characteristics for Mode I Interlaminar and Intralaminar Fractures of Cross-Ply Carbon/Epoxy Composite Laminates Based on Energy Release Rate," *Composites Research*, Vol. 32, 2019, pp. 6-12.
 10. Bianchi, F., *Numerical Modelling of Through-Thickness Reinforced Structural Joints*. PhD Thesis, Cranfield University, UK, 2012.
 11. Kim, C.H., Jo, D.H., and Choi, J.H., "Failure Strength of Composite T-joint Prepared Using a New 1-thread Stitching Process," *Composite Structures*, Vol. 178, 2017, pp. 225-231.
 12. Song, M.C., Sankar, B.V., Subhash, G., and Yen, C.F., "Analysis of Mode I Delamination of z-pinned Composites Using a Non-dimensional Analytical Model," *Composites Part B*, Vol. 43, 2012, pp. 1776-1784.
 13. Torayca T300 Technical Data Sheet No. CFA-001.
 14. Alfano, G., and Crisfelg, M.A., "Finite Element Interface Models for the Delamination Analysis of Laminated Composites: Mechanical and Computational Issues," *International Journal for Numerical Methods in Engineering*, Vol. 50, 2001, pp. 1701-1736.
 15. Yan, Y., and Shang, F., "Cohesive Zone Modeling of Interfacial Delamination in PZT Thin Films," *International Journal of Solids and Structures*, Vol. 46, 2009, pp. 2739-2749.
 16. Diehl, T., "On Using a Penalty-based Cohesive-zone Finite Element Approach, Part II: Inelastic Peeling of an Epoxy-bonded Aluminium Strip," *International Journal of Adhesion and Adhesives*, Vol. 28, 2008, pp. 256-265.
 17. ANSYS Documentation, Mechanical APDL. ANSYS Inc. Release 19.0. 2018.
 18. Kravchenko, S., Krsvchenko, O., Wortmann, M., Pietrek, M., Horst, P., and Pipes, R.B., "Composite Toughness Enhancement with Interlaminar Reinforcement," *Composites Part A*, Vol. 54, 2013, pp. 98-106.
 19. Bianchi, F., and Zhang, X., "A Cohesive Zone Model for Predicting Delamination Suppression on z-pinned Laminates," *Composites Science and Technology*, Vol. 71, 2011, pp. 1898-1907.
 20. Mohamed, G., Allegri, G., Yasaee, M., and Stephen, R.H., "Cohesive Element Formulation for z-pin Delamination Bridging in Fibre Reinforced Laminates," *International Journal of Solids and Structures*, Vol. 132-133, 2017, pp. 232-244.